Imperfect homoclinic bifurcations

Glendinning, Paul and Abshagen, Jan and Mullin, Tom

2001

MIMS EPrint: **2006.96**

Manchester Institute for Mathematical Sciences
School of Mathematics

The University of Manchester

ISSN 1749-9097

Imperfect Homoclinic Bifurcations

Paul Glendinning
Department of Mathematics, UMIST, P.O. Box 88, Manchester M60 1QD, UK
Jan Abshagen & Tom Mullin
Manchester Center for Nonlinear Dynamics, University of Manchester, Oxford Road, Manchester M13 9PL, UK

(Dated: March 26, 2001)

Experimental observations of an almost symmetric electronic circuit show complicated sequences of bifurcations. These results are discussed in the light of a theory of imperfect global bifurcations. It is shown that much of the dynamics observed in the circuit can be understood by reference to imperfect homoclinic bifurcations without constructing an explicit mathematical model of the system.

PACS numbers: 02.30.Oz,05.45.-a,05.45.Gg
Keywords: gluing bifurcations, experiments, theory, almost symmetric systems

I. INTRODUCTION

The rôle of symmetries in determining the behaviour of nonlinear physical systems can be crucial. Reflection (or $\mathbf{Z}_2$) symmetry is relevant to a wide range of experiments, and in such a system a pair of stable solutions may be created by a supercritical pitchfork bifurcation as a parameter is varied. These new states break the original symmetry, but are symmetric images of each other. Of course, perfect symmetry is never achievable in any physical system so in practice the bifurcation may become disconnected having one branch which varies monotonically with the parameter and a second which arises by a saddle–node bifurcation. This is most easily modelled by adding an imperfection term as a constant in the model normal form and this appears to work well in describing the local bifurcation structure. However, a physical system will typically contain many sources for this imperfection and some of them may be high–dimensional in nature. Therefore, it is reasonable to ask whether a model with a single imperfection term provides a good representation of the system far from the bifurcation point. Specifically, we are interested here in the effects of this local modelling on the global dynamics which result from homoclinic bifurcations.

Our investigation is concerned with a class of global bifurcations involving homoclinic orbits, i.e. orbits which tend to a stationary point of the model flow in both forwards and backwards time. Typically, the existence of a homoclinic orbit is not a persistent property of a differential equation, but they occur on lines in two-parameter families (technically, they are codimension one bifurcations). In the absence of symmetry, the net effect of such bifurcations is to create or destroy a periodic orbit, whose period tend to infinity at the bifurcation point. This may happen in one of two ways: one-sided or two-sided. In the one-sided case, the orbit apporaches the bifurcation point from one side of the bifurcation point as its period tends to infinity. In the two-sided case, such as the Shil'nikov case [1], the locus of the orbit in parameter space oscillates about the bifurcation value creating the so–called 'Shil'nikov wiggle' as the period of the orbit tends to infinity. Moreover, there are period-doubling and reverse period-doubling bifurcations of the orbit together with more complicated homoclinic bifucations. This sequence of events has been reported previously [2] in an experimental and theoretical study of a modified van der Pol oscillator, and in a wide variety of other experiments including Taylor–Couette flows [3, 4], optics, [5, 6], chemical oscillators [7, 8] and liquid crystal flows [9].

In the presence of simple symmetries, homoclinic bifurcations may involve two or more homoclinic orbits. In the simplest cases the net effect is to destroy a pair of periodic orbits which are the image of each other under the symmetry and create a single symmetric branch of periodic orbits. These symmetric periodic orbits cannot undergo period-doubling bifurcations in the two sided case. The period-doubling and reverse period-doubling bifurcations on branches of the symmetric orbit are replaced by an initial symmetry-breaking (or reverse symmetry-breaking) bifurcation. The asymmetric orbits created in this way may, of course, be involved in period-doubling bifurcations. This distinction will be useful in the interpretation of the bifurcations observed below.

Whilst the effect of small symmetry-breaking terms on the bifurcations of stationary solutions has a long history (the imperfection theory of Golubitsky and Schaeffer [10–12]) there appears to have been no systematic attempt to describe the equivalent modifications of global bifurcations (although see [13, 14] for a special case). Our aim here is to provide the foundations for such an approach. We reconsider the experimental electronic oscillator [2] which exhibits a variety of almost symmetric global bifurcations and show how many features observed in the experiments may be explained by reinterpreting some results on codimension two homoclinic bifurcations so as to

obtain a general imperfection theory for homoclinic bifurcations. These results necessarily involve non-stationary solutions, and so are likely to be applicable and observable in many more interesting situtations.

The experiments were carried out using a van der Pol oscillator. The bifurcation structure of this system has been investigated in detail previously [2] but with the implicit assumption of symmetry. It is the aim of the present study to investigate the global dynamics of the circuit and relate the observations to modern ideas on gluing bifurcations where the mathematical abstraction of perfect symmetry is relaxed.

II. EXPERIMENT I

A. The electronic oscillator

The experimental study was performed using a van der Pol oscillator circuit, the details of which are given in Healey et al. [2]. It comprises an autonomous LCR oscillator with two nonlinear conductances in the feedback circuit. Precise variation of the two parameters which control the behaviour of the system was provided by switchable decades resistance boxes. By this means determination of the bifurcation structure to a relative accuracy of better than 0.1% was possible. The two parameters are denoted by α_1, β_1 and they are nondimensionalised forms of the resistances R_1, R_2 which control the nonlinear elements. Details of the nondimensionalisation are given in Healey et al. [2].

The principle set of observations were made using an oscilloscope. Steady bifurcations were observed as changes in the level of the d.c. output. On the other hand dynamical states were best monitored as Lissajous figures formed from a combination of signals measured over the nonlinear elements. In this way, limit cycles, period doubling sequences, chaos etc. were readily displayed. Time-series were also recorded and stored on a computer via a 12-bit A/D for further processing. This included phase portrait analysis using the method of delay coordinates.

The inductor used in the present circuit is 1.5269H compared with 1.78H used by Healey et al. [2]. This causes a shift of the bifurcation points relative to those previously reported, though the bifurcation structure remains qualitatively the same. The imperfections in the circuit are tiny and the resulting disconnections are equally small. They arise from a variety of sources but we will refer to them throughout as a single imperfection.

B. Bifurcation set

The stability diagram for the electronic circuit is shown in Figure 1. The overall structure shows lines of steady and dynamic bifurcations all meeting at the top right hand corner of the figure which is a codimension–2 point.

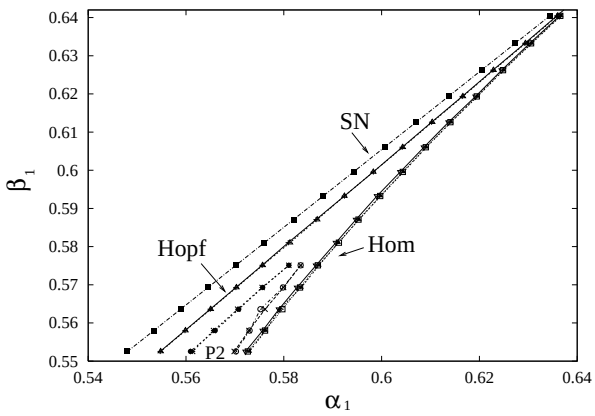

FIG. 1: Experimental bifurcation set in the α_1, β_1 plane. SN denotes the path of saddle-node bifurcations, 'Hopf' the Hopf bifurcations to simple oscillations and 'Hom' the gluing bifurcations. The paramater region denoted by 'P2' is where forward and reverse period doubling is observed on the asymmetric orbits.

The dynamic bifurcations (Hopf and homoclinic) are pairs of lines superposed and separated by the imperfections in the circuit. This effect is very small and cannot be resolved on the scale of the figure but, as we will show below, it has a significant effect on the global dynamics.

In the parameter range of interest, a perfectly symmetric system would have a trivial zero volts fixed point which would lose stability to a pair of non–zero d.c. states at a supercritical pitchfork bifurcation. As expected, in the experiment we see that this bifurcation is disconnected to form a continuously connected state and a separate solution branch which is terminated at its lower end by a saddle–node bifurcation denoted by SN in Figure 1. The stable non-trivial asymmetric d.c. states both become time-dependent via Hopf bifurcations; one on each branch. The imperfection in the circuit is very small, so the loci of these bifurcations almost coincide and are marked 'Hopf' in Figure 1. The two asymmetric limit cycles which arise at the Hopf bifurcations appear to glue together leading to a large symmetric periodic orbit. This transition is denoted by the line marked 'Hom' in Figure 1 and will be discussed in detail below. This symmetric limit cycle undergoes different types of bifurcation including symmetry-breaking and period doubling and may also become chaotic. Finally, within the oscillatory regime forward and reverse period doubling sequences have been observed and these can be related to the Shil'nikov wiggle as shown by Healey et al [2]. The boundaries of this region are denoted by P2 in Figure 1.

C. Imperfect gluing bifurcation

We first examine the influence of the imperfection on the gluing bifurcation which occurs when the two asymmetric limit cycles join without the presence of compli-

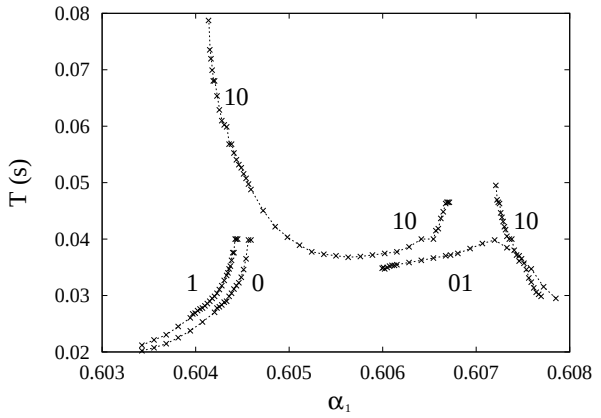

FIG. 2: Oscillation period of different periodic orbits at $\beta_1 = 0.6000$ plotted as a function of α_1. '1' and '0' denote the orbits on the asymmetric branches and '10', '01' are the glued orbits.

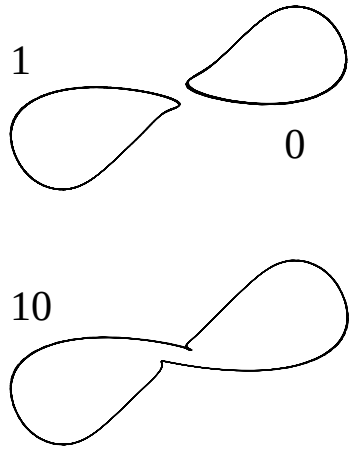

FIG. 3: Phase portraits of coexisiting asymmetric $(1, 0)$ and symmetric (10) periodic orbits at $\alpha_1 = 0.6041$ and $\beta_1 = 0.6000$

cated dynamics. We chose β_1 sufficiently large ($\beta_1 \geq 0.59$ approximately) and α_1 close to β_1 so that the chaos which arises from period-doubling sequences on a Shil'nikov wiggle is avoided and the dynamics is almost planar. We present a 'typical' set of results for the orbit structure of the oscillator in this regime in Figures 2 and 3 which were taken at $\beta_1 = 0.6000$. Figure 2 shows the period of the various simple orbits observed as a function of the parameter α_1, and Figure 3 shows the form of the corresponding orbits – the two small asymmetric orbits are labelled by '1' and '0' respectively, and the large amplitude orbit is labelled by '10', for reasons which will be explained below.

If the electronic oscillator were symmetric then the development of the orbits shown in Figure 3 for $\alpha_1 = 0.6041$ would have a simple explanation in terms of gluing bifurcations [15]: two periodic orbits which are the symmetric image of each other approach a stationary point and are 'glued together' to form the single symmetric orbit with code '10'. At the bifurcation the two smaller periodic orbits touch at the stationary point, i.e. they are no longer periodic (their period has diverged to infinity) and they form two homoclinic orbits, biasymptotic to the stationary point.

As is clear from Figure 2, and as should be expected of a real physical system, the oscillator is not perfectly symmetric. Hence it is not surprising that the pair of homoclinic orbits which exist at a single parameter value in the symmetric system seem to occur at different parameter values in the oscillator. The results shown in Figure 2 also suggest that there is a third homoclinic bifurcation – the bifurcation which creates the large amplitude '10' periodic orbit.

It can be seen in Figure 2 that the period of both the small asymmetric orbits '1' and '0' increases as α_1 increases and they finally lose stability and jump to the '10' orbit at $\alpha_1 \approx 0.6045$ i.e. where the graphs of the variation of period are almost vertical. Moreover, the '0' orbit remains stable for slightly higher values of α_1 than the '1' orbit, emphasising that the two orbits are not the images of each other under the symmetry. It should be noted that the '1' orbit results from a Hopf bifurcation on the monotonic branch of the disconnected pitchfork bifurcation. Therefore it loses stability before the '0' orbit. This is precisely what is predicted by the addition of a constant term to the normal form. The orbits shown in Figure 3 all coexist at $\alpha_1 = 0.6041$ and are typical examples of the limit cycles involved in this gluing bifurcation. The fact that they can all coexist explains why hysteresis can be observed in the experiments.

There are three features in Figure 2 which we will seek to explain theoretically in the next section: the break up of the gluing bifurcation, hysteresis, and also the extra bifurcations evident at larger values of α_1. Before describing the theory we shall look at this latter sequence of bifurcations in more detail.

D. Symmetry-breaking bifurcation of large periodic orbit

It is known that symmetric systems cannot undergo period–doubling sequences directly [16] but must first break their symmetry. Hence, we would expect the large symmetric orbit formed by the gluing of the two asymmetric ones will suffer a symmetry breaking bifurcation, as predicted for the symmetric Shil'nikov wiggle [17]. This was observed at $\beta_1 = 0.6000$ for α_1 just above 0.6059. The bifurcation was detected by measuring the mean voltage averaged over 150 periods of the oscillation and plotting this as a function of α_1. The resulting bifurcation diagram is shown in Figure 4 where we see that it has the form of a disconnected pitchfork. This diagram explains the creation of the orbit labelled '01' in Figure 2. Note that the original '10' orbit has a larger period but

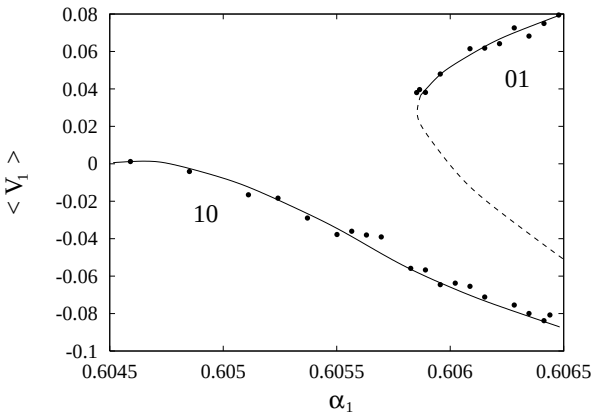

FIG. 4: Bifurcation diagram of symmetry-breaking bifurcation of periodic orbits at $\beta_1 = 0.6000$. The mean of V_1 over 5000 data points is plotted.

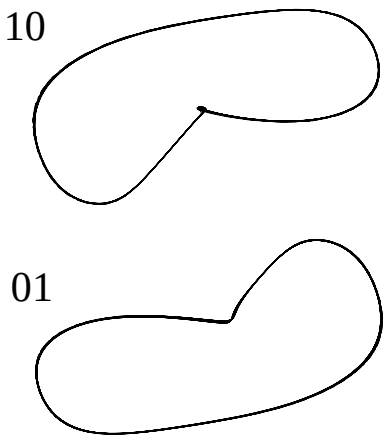

FIG. 5: Phase space portrait of coexisiting "large" periodic orbits 10 and 01 at $\beta_1 = 0.6000$ and $\alpha_1 = 0.6067$

smaller $< V_1 >$ than the newly created '01' orbit and so the branches in Figures 2 and 4 are apparently reversed. Two typical asymmetric orbits on respective branches are shown in Figure 5 for $(\alpha_1, \beta_1) = (0.6067, 06000)$. It is evident that the '10' orbit on the connected branch displays strong variation in period for $\alpha_1 > 0.6065$ and then instability. However, the '01' orbit is virtually constant over this range. Both orbits then show reduction in period for high α_1 values. Each orbit undergoes period doubling sequences to chaos for α_1 values greater than the range displayed in Figure 2. The extra complications of period doubling and instability are topics for future research.

III. THEORY

It is natural to think of the bifurcations observed in the system in terms of two parameters. One of these, μ say, is the parameter of the (fictional) symmetric system which has a gluing bifurcation as described in section II C. The second parameter, ϵ say, is a measure of how far the oscillator is from being perfectly symmetric, i.e. it is some measure of imperfection with $\epsilon = 0$ corresponding to the perfectly symmetric system. Just as the standard imperfection theory for the bifurcations of stationary points [12] allows one to describe the effect of asymmetry in terms of μ and ϵ, our aim here is to give an analogous description for general global bifurcations. We note that this is in the spirit of the work of Glendinning [14] and Cox [13] for the particular case of Lorenz-like bifurcations.

A. The basic picture

Suppose that $(\mu, \epsilon) = (0, 0)$ denotes the point in parameter space at which there are two symmetrically related homoclinic orbits. Consider either one of these orbits. Since the existence of homoclinic orbits is codimension one, there will be a curve in parameter space through $(0, 0)$ on which systems have a homoclinic orbit which is a continuation of the given orbit. Thus, for typical two-parameter families of systems, there will be two curves of homoclinic orbits in parameter space, G_0 and G_1 say, which intersect at the origin and which do not intersect the line $\epsilon = 0$ again locally. The curve G_0 (respectively G_1) is the locus of a homoclinic bifurcation which creates or destroys the periodic orbit with code 0 (respectively, 1). The one-parameter families of nearly symmetric systems such as the example considered in the previous section would then correspond to some curve in this two parameter space which has, for example, $\epsilon > 0$ and which passes close to $(\mu, \epsilon) = (0, 0)$. Such a curve will intersect both G_0 and G_1, but at different parameter values, so there will be two simple homoclinic bifurcations at nearby parameter values on such a path.

The intersection of the loci of two homoclinic bifurcations (each to the same stationary point) is a codimension two phenomenon which has been studied by a number of authors[15, 18–24]. The most important feature which all these bifurcations have in common is that at least two other curves of homoclinic orbits emanate from the intersection of G_0 and G_1, one in $\epsilon > 0$, labelled G_{10}, and the other in $\epsilon < 0$ labelled G_{01}. The labelling describes the order (in time) that the orbit passes through neighbourhoods of the basic homoclinic orbits. These homoclinic orbits are precisely the bifurcations needed to destroy or create (asymmetric) periodic orbits with code '10' or '01'. Thus a typical path close to $\epsilon = 0$ will intersect G_0, G_1 and one of the curves G_{01} or G_{10}. This explains the third homoclinic bifurcation observed in Figure 2. Roughly speaking, the difference between orbits created by paths crossing G_{10} and those created by crossing G_{01} is the difference between the orbits shown in Figure 5.

The details of the two-parameter bifurcation plane

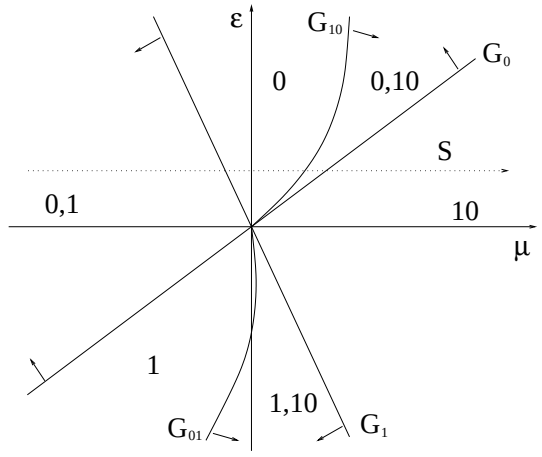

FIG. 6: The two parameter plane for the imperfect gluing bifurcation in the planar case. A one parameter family of (imperfect) systems, S, is indicated by a curve through the plane close to $\epsilon = 0$. The arrows indicate the direction in which orbits are created.

close to the intersection of G_0 and G_1 depends upon the nature of the stationary point, the configuration of the homoclinic orbits and a measure of the amount of twisting of solutions about these orbits. The nature of the stationary point is determined by the eigenvalues of the Jacobian matrix of the flow which are closest to the imaginary axis. If, up to complex conjugation, these are λ_1 and λ_2 with $\mathrm{Re}\ \lambda_1 < 0 < \mathrm{Re}\ \lambda_2$ then the *saddle index*, δ, defined by

$$\delta = -\mathrm{Re}\ \lambda_1 / \mathrm{Re}\ \lambda_2 \tag{1}$$

plays an important role. The two-parameter space near the intersection of G_0 and G_1 in the planar case is shown in Figure 6 (λ_1 and λ_2 are real), where the symmetry is a point symmetry about the stationary point and the direction of time may be chosen so that $\delta > 1$. Each simple homoclinic bifurcation creates a periodic orbit in the direction indicated by the arrow on the bifurcation curve. The parameter plane is divided into six regions by the curves of bifurcations, and the periodic orbits (from the local theory) which exist in each region are indicated by their codes. The bifurcations observed on the one-parameter path S in Figure 6 are shown in Figure 7, which is the more conventional representation.

B. Relationship with the experiment

The curves sketched in Figure 7 are in reasonably good agreement with the experimental ones in Figure 2 except for the extra complications at larger parameter values described in section II D. Also the fact, mentioned at the end of section II C, that all three of the orbits labelled '0', '1' and '10' coexist for some values of α_1. However, even these aspects can be incorporated into our picture of imperfect global bifurcations. For smaller values of β_1

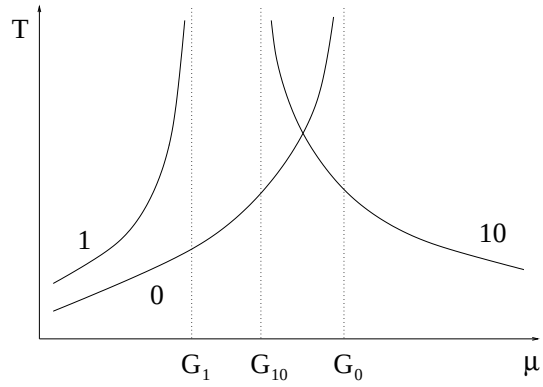

FIG. 7: Bifurcation diagram (period against parameter) on the one-parameter path S of Figure 6.

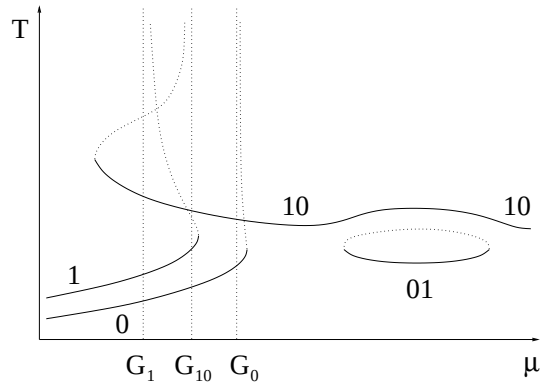

FIG. 8: Bifurcation diagram (period against parameter) of the modified global bifurcation as suggested by Figure 2.

Shil'nikov wiggles are observed, suggesting that $\delta < 1$ (and λ_1 is complex) in this parameter regime. In this case, as earlier, there may be symmetry-breaking and reverse symmetry-breaking bifurcations of the symmetric orbit (in the perfectly symmetric system) [17]. The bifurcations observed in Figure 2 and described in more detail in Figure 4 are not in the asymptotic region of applicability of the homoclinic theory (large period, close to homoclinic bifurcation) and so we invoke an extra pair of assumptions on the underlying symmetric system for our model: that there is a symmetry-breaking and reverse-symmetry breaking bifurcation on the symmetric orbit and that $\delta < 1$.

If $\delta < 1$ then the curves of homoclinic bifurcations are essentially as in Figure 6 but the direction of the bifurcations is reversed (more precisely, the diagram is reflected about the $\epsilon-$axis) and the orbits created are saddles (rather than stable, as would be the case if $\delta > 1$). This now suggests the new interpretation of Figure 2 which is shown in Figure 8. The major new feature is that since the orbits are created in the opposite direction to the case with $\delta > 1$ in Figure 6 and are unstable, the points at which the orbits cannot be followed further ($\alpha_1 = 0.6041$ for the '10' orbit and $\alpha_1 = 0.6025$ for the '0' and '1' orbits in Figure 2) are now assumed to be saddle–node bifurca-

tions. There are a number of possible interpretations for the disconnected symmetry–breaking bifurcations, and one of these is shown in Figure 8, although we make no claim that it is the most likely. Note that the new arrangement of the homoclinic bifurcations does provide a region of parameters where the orbits '0', '1', and '10' coexist and are stable, as seen in the experiment.

The important feature of the analysis above is that two assumptions about the underlying mathematical model are sufficient to explain the orbits observed in the experiment. It is worth emphasising that this can be done *without* constructing the model equations explicitly, simply be suggesting that any model equation must have various dynamical features.

C. Other cases

In the literature, codimension two global bifurcations are generally described with G_0 and G_1 as the coordinate axes of the bifurcation analysis. In this case the symmetric system may be assumed to lie on the diagonal of the parameter space, with the asymmetry parameter perpendicular to the diagonal (just tilt the diagrams by 45° to get an impression of the locus of bifurcations). It is, however, important to bear in mind that the curves G_0 and G_1 appear to intersect with a very small angle of intersection in asymmetric perturbations of symmetric systems, whereas the standard analysis depicts the intersection angle to be at right angles. Provided the intersection is transversal the analysis is not affected, although it does mean that the true picture for the asymmetric perturbation will be a very skewed version of the standard pictures.

The basic feature common to all the relevant types of bifurcation we consider is that as the bifurcation parameter μ is varied, a (more or less complicated) sequence of bifurcation is observed with the net effect that a pair of periodic orbits (those we have labelled '0' and '1') is destroyed, and a single large periodic orbit is created. The precise details of the bifurcations depends on the system, but it is still possible to make a number of general statements.

1 *The one-sided case*

If the direction of time can be chosen so that λ_2 is real and $\delta > 1$ (cf. (1)) then the codimension one bifurcations on G_0 and G_1 are one-sided and fairly general statements about the bifurcations involved *in the range of validity of the rigorous argument: large period and parameters close to the intersection of* G_0 *and* G_1 are possible [22]. First, there are at most two periodic orbits, and second, any periodic orbit has a very particular description in terms of the symbols '0' and '1' introduced above. Technically, the sequences are rotation compatible sequences [22], but in practice a simple consequence is that periodic orbits have codes of the form

$$01^{n_1}01^{n_2}01^{n_3}01^{n_4}01^{n_5}\dots \tag{2}$$

where for all i, $n_i \in \{m, m+1\}$ for some $m > 0$ (or the same with the roles of 0 and 1 exchanged). Moreover, the limit, ρ, of the number of $1s$ in the sequence to the length of the sequence exists and is called the rotation number of the orbit. In one case (the so-called stable orientable Lorenz-like case, see [21]), there is an infinite set of bifurcations along a typical path and at any one parameter after crossing the first bifurcation curve, there is at most one periodic orbit. Moreover, the rotation number varies continuously along the bifurcation path, implying the existence of parameter values with non-periodic (but non-chaotic) attractors.

If λ_1 is complex then the range of bifurcations is more complicated and depends on the precise path taken through the parameter space. Here there are regions of coexistence of certain periodic orbits – those whose rotation numbers $\frac{p_1}{q_1}$ and $\frac{p_2}{q_2}$ are Farey neighbours, i.e. $|p_1q_2 - q_1p_2| = 1$ – but typical curves in parameter space do not intersect most of these regions. A more complete list of the possibilities can be found in [17, 18, 21].

All the bifurcations of the rigorous analysis involve one-sided global bifurcations, and there are no local bifurcations on the branches of each periodic orbit. If these occur it is necessary to appeal to effects outside the rigorous region of validity of the mathematical results – this is made much easier by an understanding of the two-sided bifurcations.

2 *The two-sided case: Shil'nikov's wiggle*

The symmetric bifurcation diagram of the Shil'nikov case (λ_1 complex, λ_2 real and $\delta < 1$) is given in [17]. The locus of the pair of orbits ('0' and '1') in parameter-period space oscillates as the period increases to infinity, with period-doubling and reverse period-doubling bifurcations on every other branch. The symmetric orbit oscillates in a similar way, but with symmetry-breaking bifurcations on every other branch. Breaking the symmetry of the system will have two effects – the global bifurcations which coincide in the symmetric system will be split apart and the symmetry-breaking bifurcations will typically become disconnected as described above. In the two–parameter diagram close to the intersection of G_0 and G_1, curves of more complicated bifurcations (G_{01} and G_{10}) oscillate rapidly and intersect each other (there are infinitely many other curves of homoclinic bifurcations to complicate matters further). For a typical asymmetric path there will be a single intersection with G_0 and G_1, but potentially several intersections with G_{10} and G_{01}. The orbits created in the bifurcations involving G_0 and G_1 will lie on the usual Shil'nikov wiggle in the parameter–period plane as observed experimentally (see

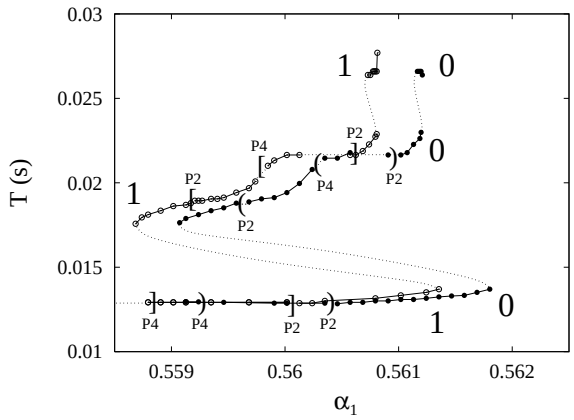

FIG. 9: Coexisiting Shil'nikov wiggle at $\beta = 0.5317$. The branch noted with [ ] correspond to the '1' and with ( ) to the '0' orbit respectively.

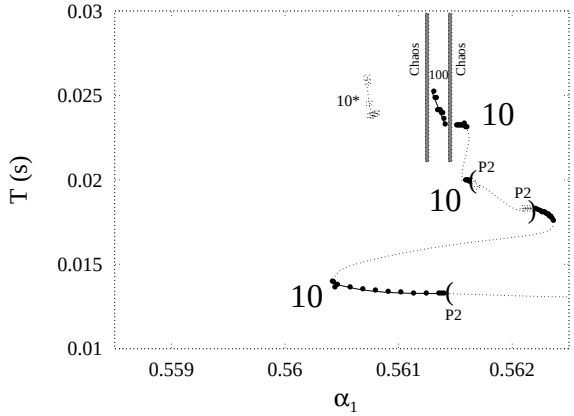

FIG. 10: Shil'nikov wiggle and gluing process of the '10' orbit at $\beta = 0.5317$. The period of the '10' orbits and the '100' orbit is rescaled by two and three respectively.

Figure 9). The symmetric orbit, '10', can also be followed experimentally (see Figure 10); there are multiple intersections of the parameter path with G_{10}, i.e. extra bifurcations which create and destroy the orbits labelled '10*'. Between the conjectured intersection of the parameter path with G_0 and G_{10} it is possible to observe a stable orbit with code '100'. Such an orbit can be created from homoclinic orbits obtained from the gluing of the orbits '10' and '0'. These bifurcations are expected due to the intersection of G_0 and G_{10} in the two parameter analysis (cf. the $\delta > 1$ case in [22]) which create extra curves of homoclinic orbits G_{010} and G_{100}.

IV. EXPERIMENT II

The gluing process in the non–planar region of parameter space involves complicated orbits which evolve on a Shil'nikov wiggle. A pair of these wiggles are shown

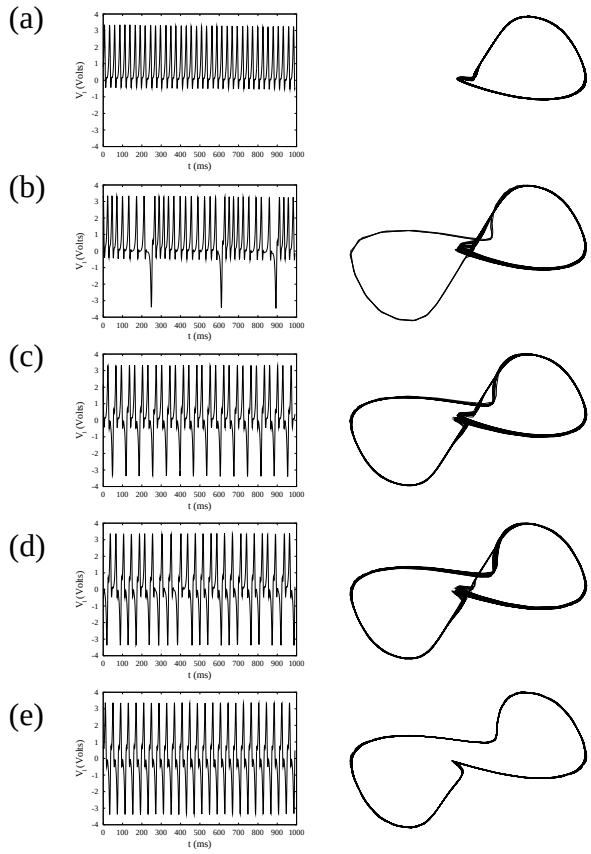

FIG. 11: Time series and phase portraits of different dynamical states involved in imperfect gluing bifurcation at $\beta = 0.5317$. (a) periodic orbit '0' on asymmetric branch at $\alpha_1 = 0.56119$, (b) chaos at $\alpha_1 = 0.56125$, (c) period-3 orbit '100' at $\alpha_1 = 0.56136$, (d) chaos at $\alpha_1 = 0.56146$, (e) symmetric periodic orbit '10' at $\alpha_1 = 0.56152$

in Figure 9 where the period is plotted as a function of α_1 at fixed $\beta_1 = 0.5317$. Here the period of the orbit approaches infinity through a sequence of folds where alternate branches are unstable and indicated by dashed schematic lines in the figure. The stable solutions undergo forward and reverse period–doubling sequences on the first two folds whereas the highest period orbits only exist over a tiny range of the parameter.In a perfectly symmetric system these two wiggles would overlap completely. The effect of the imperfection in the circuit is to displace the two curves from one another.

A Shil'nikov wiggle has also been observed on the symmetric orbit and the results are shown in Figure 10. There we can see three levels of the wiggle with period doubling sequences. The '10' orbits in this case were asymmetric but we were unable to find the mirror image pairs of solutions in this case. We were, however, able to observe them at smaller values of β_1. The gluing process takes place on the third level with intervening sequences of chaos and a stable '100' orbit; as expected from the discussion at the end of section III C. Note we also observed the '10*' which is an integral part of the gluing process

as discussed in section III C above. A set of time–series and phase portraits are displayed in Figure 11. The '0' orbit on the disconnected branch glues to the '10' large scale orbit via two chaotic phases with an intermediate period–3 '100' sequence.

V. CONCLUSION

Although symmetric equations are frequently used to model almost symmetric systems, we have shown that a more careful examination of experiments can reveal features which do not appear in the symmetric models. In particular, we have focussed here on global bifurcations which involve periodic states of the system, and we have shown how a number of complicated bifurcation diagrams observed in the experiments can be interpreted by appealing to a theory of imperfect homoclinic bifurcations.

A standard approach to the modelling of physical phenomena is to construct a mathematical model of the experiment, and use this to either predict or explain features of the experiment. This entails both the construction of the model and the analysis of the model constructed. It is noticeable that in the approach taken here we have appealed to properties of a model *without* having to either construct or analyse the model. We have simply said that any mathematical model of the experiments must have certain features, and that these features lead to certain conclusions by the application of global bifurcation theory.

Bifurcation diagrams consistent with those of section III have now been observed in more physically interesting systems. Abshagen [25] has found bifurcation diagrams with a striking similarity to Figure 6 in experimental data from fluid flow. We believe that the approach taken here will find application in a broad variety of experiments in which symmetry, or rather, almost-symmetry, plays a role.

REFERENCES

[1] P. Glendinning 'Stability, Instability and Chaos' (CUP) 1994.

[2] J.J. Healey, D.S. Broomhead, K.A. Cliffe, R. Jones and T. Mullin (1991) Physica D **48**, 322-339.

[3] T. Mullin and T.J. Price (1989) Nature **340**, 294-296.

[4] J. von Stamm, U. Gerdts, T. Buzug and G. Pfister (1996) Phys. Rev. E **54**, 4938-4957.

[5] E. Allaria, F.T. Arecchi, A. Di Garbo and R. Meucci (2001) Phys. Rev. Lett. **86**, 791-794.

[6] R. Herrero, R. Pons, J. Farjas, F. Pi and G. Orriels (1991) Phys. Rev. E **53**, 5627-5636.

[7] M.J.B. Hauser and L.F. Olsen (1996) J. Chem. Soc. Far. T. **92**, 2857-2863.

[8] A. Arnéodo, F. Argoul, J. Elezgaray and P. Richetti (1993) Physica D **62**, 134-169.

[9] T. Peacock and T. Mullin (2001) J. Fluid Mech. **432**, 369-386.

[10] M. Golubitsky and D. Schaeffer (1979) Comm. Pure Appl. Math. **32**, 21-98.

[11] M. Golubitsky and D. Schaeffer (1979) Comm. Math. Phys. **67**, 205-232.

[12] D. Schaeffer (1981) in *Dynamical Systems and Turbulence*, eds. D.A. Rand and L.-S. Young, Springer LNM 898, Berlin.

[13] S.M. Cox (1991) J. Fluid Mech. **227**, 1-33.

[14] P. Glendinning (1987) Dyn. Stab. Syst. **2**, 43-53.

[15] P. Coullet, J.-M. Gambaudo and C. Tresser (1984) C.R. Acad. Sci. (Paris), Série I, **299**, 253-256.

[16] J.W. Swift and K. Wiesenfeld (1984) Phys. Rev. Lett. **52**, 705-708.

[17] P. Glendinning (1984) Phys. Lett. A **103**, 163-166.

[18] J.-M. Gambaudo (1987) Thesis, Université de Nice.

[19] J.-M. Gambaudo, P. Glendinning and C. Tresser (1984) C.R. Acad. Sci. Série I, **300**, 311-313.

[20] J.-M. Gambaudo, P. Glendinning and C. Tresser (1985) J. Physique Lett. **46**, L653-L658

[21] J.-M. Gambaudo, P. Glendinning and C. Tresser (1987) 'Stable cycles with complicated structures' in *Instabilities and nonequilibrium structures*, eds. E. Tirapegui and D. Villarroel, D.Reidel Publishing Co.

[22] J.-M. Gambaudo, P. Glendinning and C. Tresser (1988) Nonlinearity **1**, 203-214.

[23] D.V. Lyubinov, A.S. Pikovsky and M.A. Zaks (1989) Sov.Sci.Rev.C.Math.Phys. **8**, 221-292

[24] D.V. Turaev and L.P. Shil'nikov (1986) Dokl.Akad.nauk SSSR **290** 1301-1304

[25] J. Abshagen, G. Pfister, T. Mullin (In preparation)